JOURNAL OF APPLIED ELECTROCHEMISTRY 23 (1993) 728–734

Electrochemical and oxygen reduction behaviour of solid silver–bismuth/antimony electrodes in KOH solutions

I. ARUL RAJ, K. I. VASU

Central Electrochemical Research Institute, Karaikudi, 623 006, India

Received 24 February 1992; revised 23 June 1992

Oxygen reduction behaviour at silver–low bismuth/antimony electrodes was investigated by electrochemical methods in KOH solutions. The electrochemical redox characteristics such as peak multiplicity, peak currents and peak potentials on these electrodes under both potentiostatic steady state and cyclic voltammetric conditions were obtained. The anomalies associated with the redox peak potential values both in the anodic and cathodic branches of the cyclic voltammograms were attributed to the distinct electrochemical behaviour of bismuth/antimony on the electrode surface along with silver. The behaviour of these electrodes for the electrocatalytic cathodic reduction of oxygen was also investigated both by potentiostatic steady state and cyclic voltammetric techniques under rotating conditions. The kinetic parameters corresponding to the electrochemical reduction of oxygen on these electrodes were obtained. These electrodes were ranked with respect to their electrocatalytic activity both for the oxygen reduction and evolution reactions.

1. Introduction

Electrochemical investigations on silver electrodes in alkaline solutions arise from fundamental and practical interests [1–3]. Silver is a known electrocatalyst for the reduction of oxygen in alkaline fuel cell cathodes. Several research papers [4, 5] have dealt with the reduction of oxygen on silver electrodes. The apparent anomalies in the oxygen reduction currents on silver under such conditions were attributed to the existence of monolayers of Ag_2O oxide at potentials more cathodic than the Ag/Ag_2O reversible potential [6]. It was also reported [7] that silver containing very low percentages of nickel/titanium/bismuth was electrocatalytically very active for the oxygen reduction reaction in alkaline solutions. The electrodes investigated in [6] were smooth solids whereas those in [7] were premixed powder coatings obtained on suitable bases, using binders. In this work, however, silver containing 2 to 5 at % Sb and 2 to 5 at % Bi was fabricated as smooth solid disc electrodes.

The electrochemical redox characteristics of these electrodes in KOH solutions were obtained with a view to comparing the values of the redox peak characters under cyclic voltammetric conditions with those of pure silver. The oxygen reduction behaviour of these electrodes was examined to study the influence of bismuth/antimony on the anomalies associated with the oxygen reduction currents on silver. Moreover, it was desired to know whether it is possible to enhance the electrocatalytic activity of silver by alloying with bismuth/antimony for the oxygen reduction reaction with a view to application in alkaline fuel cells.

2. Experimental details

2.1. *Fabrication of test electrodes*

The test electrodes were small pieces of the alloys obtained by melting respective metal powers (Johnson Matthey, 99.99% purity) premixed in specific proportions by atomic weights and kept in an alumina boat with a resistance heating furnace under an argon atmosphere at a temperature of 970 °C, followed by annealing under argon. This procedure was repeated three times to ascertain homogeneity. The resulting melts were cut into pieces and set in glass tubes using an alkali-resistant epoxy compound so that one end formed the surfaces of the 0.12 cm^2 discs. For the rotating disc electrode experiments, the alloy melts were machined to cylindrical shape and housed in suitable holders made from Teflon rods. This arrangement provided 0.3 cm^2 disc electrodes. Electrical contacts were provided by means of silver wires and conducting silver paste or by copper rods with threads for the purpose of rotation. The electrode surfaces were polished mechanically by a four-stage polishing routine to a mirror finish with emery polishing paper (John Oakey and Sons Ltd) and degreased with acetone. This was followed by etching in hot 10% HNO_3 to remove any embedded particles. Then the surfaces were washed thoroughly with triply distilled water and housed in a standard three-compartment glass cell containing the electrolyte solution (KOH), reference electrode (Hg/HgO, OH^-) and a large surface area Pt-foil counter electrode.

0021-891X

2.2. *Preparation of electrolyte*

The electrolyte solution was prepared from GR KOH pure pellets (Sarabai (M) Chemicals) in triply distilled water. This was then pre-electrolysed between two Pt-foils for over 48 h in order to eliminate all possible impurities. This brief procedure was sufficient to give reproducible results on two identical electrodes in each category.

2.3. *Equipment and techniques*

The potentiostatic steady state polarization experiments were carried out using a high power potentiostat (Wenking HP 72). The cyclic voltammetric experiments were carried out using a PAR Electrochemistry System 370–2. The oxygen gas used was 99.9% pure and was further purified by allowing it to pass through three washing columns, successively containing 10% solution of KOH to remove any CO_2, and triply distilled water to remove any alkali taken from the first column and cell electrolyte solution to presaturate the oxygen gas prior to its entry into the test cell. In obtaining the steady state polarization data, care was taken to employ different electrodes of identical composition for the anodic and cathodic polarizations. The potentials were applied in steps of 0.025 V from the open circuit potentials. The currents were steady after 3 min holding periods. The current values within the limit of 1% variation, obtained on two identical samples, were used to construct the *i–E* curves.

X-ray diffraction measurements were carried out with CuK_α radiation (20 mA, 30 kV) in the range of 10 c.p.s. at a scan rate of $2° \text{ min}^{-1}$. The derived data obtained from the diffraction patterns were compared with the data available in the ASTM sheets to identify the phases formed, if any.

3. Results and discussion

3.1. *Physical characteristics of the melts*

The weights of the melts were the same as the total weights of the individual metals taken in all cases. Distribution of the foreign metals into the silver lattice, leading to the formation of alloy phases in the cases of bismuth and antimony, is possible only if the atomic weight percentages of these metals exceed 8 at % as per the standard phase diagrams for these systems [8]. The X-ray diffraction data obtained on silver–bismuth and silver–antimony (2 at % of each) are presented in Table 1.

These data show clearly that the alloying metal exists in a pure metallic phase only and that no new alloy phase has formed within the atomic concentrations considered, namely 2 at % Bi or 2 at % Sb in 98 at % Ag.

The melts were very brittle and not very easily machinable. The brittleness of the melts was found to increase with the atomic concentrations of bismuth and antimony in silver. The melts were very bright initially but became tarnished with time when exposed to the atmosphere.

Table 1. XRD data obtained on Ag–Bi (2%)/Sb (2%) melts

Specimen	*D values (A^0) experimental*	*ASTM*	I/I_0	*hkl*	*Phase*
Ag–Bi (2%)	2.341	2.359	100	111	Ag
	2.199	2.273	38	110	Bi
	2.036	2.044	34	200	Ag
	2.019	2.030	10	105	Bi
Ag–Sb (2%)	2.332	2.359	100	111	Ag
	2.210	2.248	56	110	Sb
	2.031	2.044	52	200	Ag
	1.814	1.878	42	006	Sb

3.2. *Chemical stability of the melts*

The chemical stabilities of both silver–bismuth/antimony in hot alkaline solutions were assessed and found to be extremely good, based on the open circuit potential–time decay patterns (not shown). The slopes of the potential against log time (in hours) plots were 10 and 21 mV dec.$^{-1}$ for Ag–Bi (2%) and Ag–Sb (2%), respectively. The open circuit potential values of the electrodes considered in this work are presented in Table 2.

3.3. *Electrochemical steady state behaviour*

3.3.1. Anodic polarization. The anodic potentiostatic steady state polarization behaviour of silver–bismuth/antimony (2 at % of each) electrodes in 1 M KOH at 25 °C is shown in Fig. 1. Three anodic current peaks can be observed in the polarization response of both the electrodes. The oxidation peak arising at a peak potential (E_p) of 0.375 V has a current (i_p) peak value of 6.0 mA cm^{-2} for Ag–Bi (2%) and 5.7 mA cm^{-2} for Ag–Sb (2%) electrodes. Since the E_0 value of the isAg/Ag_2O couple is 0.347 V vs NHE at pH 14, and the i_p values of the initial anodic peaks on both the electrodes were close to each other (the slight increase on Ag–Bi over Ag–Sb might be due to the distinct contributing influences of bismuth and antimony on the behaviour of silver; The i_p value at 0.350 V on pure silver was 6.2 mA cm^{-2}), this process has been assigned to the formation of an Ag_2O film on both the electrodes. Further anodization leads to a small peak

Table 2. Open circuit potentials of the electrodes in 1 M KOH solution at 298 K versus Hg/HgO, OH^-

Specimen	*In argon atmosphere (mV)*	*In oxygen atmosphere (mV)*
Ag–Bi (2%)	−7	+32
Ag	+71	+170
Bi	−247	−51
Sb	−370	−95
Ag–Sb (2%)	−31	+59

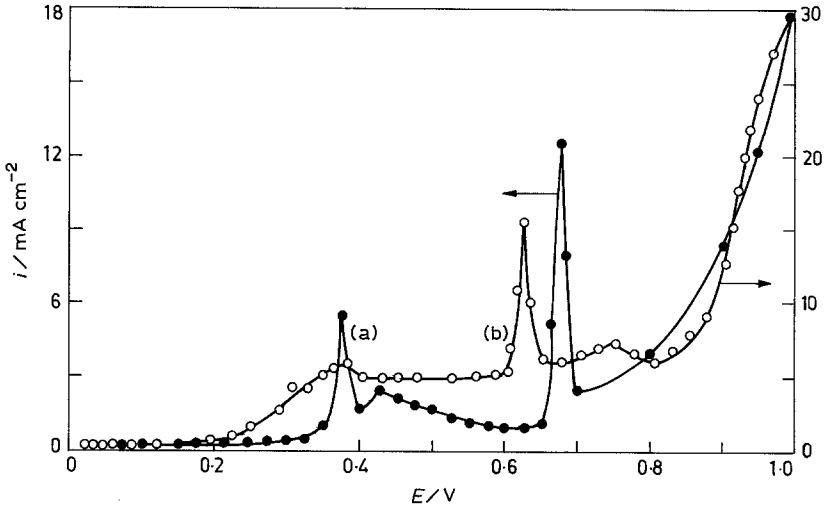

Fig. 1. The anodic potentiostatic steady state polarization curves in argon saturated 1 M KOH solution at 25 °C; (a) Ag–Sb (2%); (b) Ag–Bi (2%).

at 0.425 V only in the case of the silver–antimony alloy. Since there is no corresponding process for bismuth at this potential, this peak has been assigned to Sb_2O_3 film formation. The peak arising at 0.675 V on Ag–Sb (2%) has an i_p value of 12.45 mA cm^{-2} whereas the corresponding peak on Ag–Bi (2%) at 0.625 V has an i_p of 15.2 mA cm^{-2} (the i_p for pure silver was 16.2 mA cm^{-2} at 0.640 V).

Since this potential region corresponds to the Ag_2O/AgO redox potential value, namely 0.65 V against Hg/HgO, OH^-, this has been assigned to the oxidation of Ag_2O to AgO. The broad peak observed at 0.75 V in the case of Ag–Bi alone has been assigned to the formation of a Bi_2O_3 film, as this potential is close to the redox potential of bismuth [9]. Further anodization beyond 0.75 V leads to the evolution of oxygen. The oxygen evolution currents differ very much between these two electrodes. The current is greater on the AgO–Bi_2O_3 surface than on the AgO–Sb_2O_3 one. The shift in the peak potentials corresponding to AgO formation (0.05 V) has been attributed to the distinct but mixed influences of Sb_2O_3 in the case of the Ag–Sb electrode, and Bi_2O_3 in the case of Ag–Bi electrode. The electrochemical reactions considered for the above processes are:

$$2Ag + H_2O \rightleftharpoons Ag_2O + 2H^+ + 2e^-$$

$$2Bi + 3H_2O \longrightarrow Bi_2O_3 + 6H^+ + 6e^-$$

$$2Sb + 3H_2O \longrightarrow Sb_2O_3 + 6H^+ + 6e^-$$

and

$$Ag_2O + 2OH^- \longrightarrow 2AgO + H_2O + 2e^-$$

3.3.2. Cathodic polarization. The cathodic potentiostatic steady state polarization behaviour of Ag–Bi/Sb (2 at % of each) electrodes in 1 M KOH at 25 °C is shown in Fig. 2. The cathodic currents are much less than the corresponding anodic currents. This is because, in the potential region considered here (apart from the reduction of the oxidized species available on the surfaces), other possible reactions such as the reduction of molecular oxygen and hydrogen evolution are excluded by the proper choice of experimental conditions. Further, the cathodic currents differ little between these two electrodes. In the case of the Ag–Sb electrodes, two broad waves with $E_{1/2}$ values ~ -0.30 V and -0.50 V are obtained. In the case of Ag–Bi electrodes, two diffused peaks with E_p values ~ -0.5 V and -0.66 V are obtained. The reduction peak potential values for Sb_2O_3 and Bi_2O_3 films available at the electrode surfaces under open circuit conditions were -0.30 V and -0.66 V, respectively (Fig. 2).

When these values were compared with the corresponding oxide formation peak potential values, 0.425 V and 0.750 V, respectively, it became obvious that these redox processes were extremely irreversible, even when solid state reaction processes had been invoked to be controlling. As it was very difficult to interpret the results on these novel bimetallic electrode surfaces in terms of steady state observations, due to the relaxation time involved in the progressive growth of the oxide films formed on the electrode surfaces which were bound to be included into the measurements, linear sweep voltammetric experiments under transient conditions were carried out.

3.4. *Linear sweep voltammetric behaviour*

3.4.1. Anodic scanning. The linear sweep voltammetric curves obtained on Ag–Bi (2%) and Ag–Sb (2%) in the anodic potential scans from their open circuit potentials are shown in Fig. 3. The anodic electrochemical responses of these electrodes under transient conditions, when compared with those for steady state conditions, reveal that the peak potential for the initial oxidation processes is almost the same, i.e. 0.375 V for both the cases. The normalized charge values obtained by integration of i against $V(t)$ under these peaks amount to 2188 mC for Ag–Sb (2%) and 4219 mC for Ag–Bi (2%). The ratio of these charge values is almost 2 : 1. The i_p values amount to 4.70 mA cm^{-2} for Ag–Sb (2%) and 4.0 mA cm^{-2} for Ag–Bi (2%). A shift in the E_p value, 0.01 V under transient conditions in the case

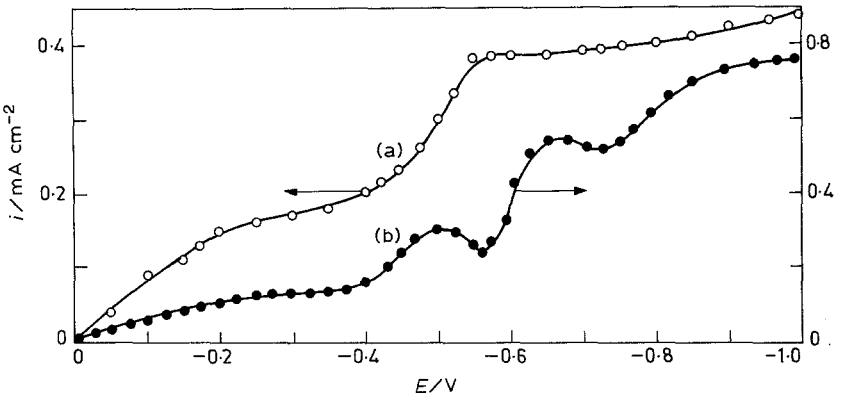

Fig. 2. The cathodic potentiostatic steady state polarization curves in argon saturated 1 M KOH solution at 25 °C; (a) Ag–Sb (2%); (b) Ag–Bi (2%).

of Ag–Bi (2%) from that of Ag–Sb (2%), is also observed.

The small peak that appears in the case of Ag–Sb (2%) under steady state conditions at 0.425 V is absent under the transient conditions. The results of repetitive experiments carried out on the same surfaces under identical conditions indicated (not shown) systematic drifts in the peak potentials and peak current densities. This suggests growth of the oxide film thickness with time and hence an estimation of it may not be accurate. The oxidation processes that occur at E_p = 0.675 V on both the electrodes have identical i_p values, i.e. 13.8 mA cm^{-2}. The normalized charge values under these peaks amount to 1402 mC for Ag–Sb (2%) and 1208 mC for Ag–Bi (2%). The ratio of these charges is approximately unity. The broad peak which occurs at 0.76 V on Ag–Bi (2%) is absent in the case of Ag–Sb (2%).

3.4.2. Cathodic scanning. The cathodic electrochemical responses of these electrodes obtained under transient conditions are shown in Fig. 4. This, when compared with those under steady state conditions, reveal that the initial reduction potential on Ag–Bi (2%) electrode is the same, i.e. −0.5 V, for both the cases. On the Ag–Sb (2%) electrode, a broad and extended peak arises at −0.5 V under transient conditions but is absent under steady state conditions. Instead, a broad wave with an $E_{1/2}$ value, at about −0.5 V appears. The second reduction peak arises on both the electrodes at −0.66 V under transient conditions. This is absent on Ag–Sb (2%) under the steady state conditions. Instead, an additional wave with an $E_{1/2}$ value −0.30 V appears. Further experiments were therefore carried out under linear sweep cyclic voltammetric conditions to analyse the redox behaviour of these electrodes in more detail.

3.5. *Cyclic voltammetric behaviour*

The linear sweep cyclic voltammetric curves obtained on Ag–Bi (2%), Ag–Sb (2%) and Ag electrodes in the potential range from −0.55 to 0.95 V are presented in Fig. 5. The anodic branch corresponding to that of silver (Fig. 5) has one small and two prominent peaks with E_p values 0.35, 0.50 and 0.825 V whereas the cathodic branch has one prominent and one small extended peak with E_p values 0.375 and 0.075 V, respectively. The anodic processes are assigned to the oxidation of Ag to AgOH at 0.35 V partially, further oxidation of Ag directly to Ag_2O at 0.50 V and to the oxidation of Ag_2O to AgO at 0.825 V [9]. Beyond 0.9 V, oxygen evolution predominates. The cathodic processes are the reverse of these anodic processes. AgO becomes reduced to Ag_2O at 0.375 V and Ag_2O to Ag at 0.075 V. The electrochemical reactions considered for the oxidation of silver are as follows:

$$Ag + OH \rightleftharpoons AgOH + e^- \quad (1)$$

$$2Ag + 2OH^- \longrightarrow Ag_2O + H_2O + 2e^- \quad (2)$$

$$Ag_2O + 2OH^- \longrightarrow 2AgO + H_2O + 2e^- \quad (3)$$

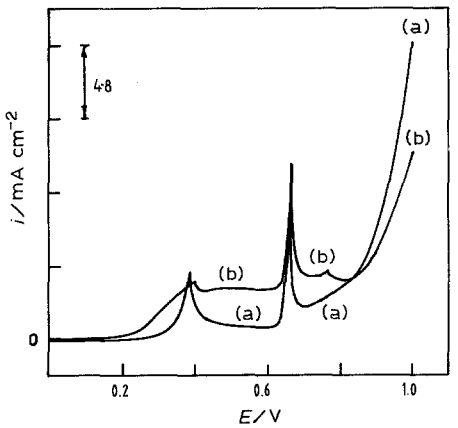

Fig. 3. The anodic linear sweep voltammetric curves in argon saturated 1 M KOH solution at 25 °C and at 1 mV s^{-1}; (a) Ag–Sb (2%); (b) Ag–Bi (2%).

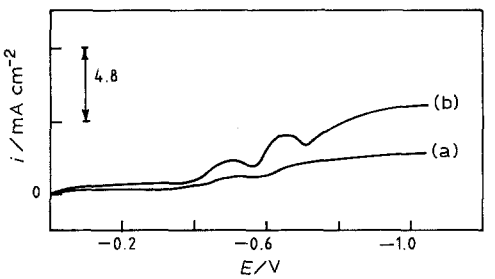

Fig. 4. The cathodic linear sweep voltammetric curves in argon saturated 1 M KOH solution at 25 °C and at 1 mV s^{-1}; (a) Ag–Sb (2%); (b) Ag–Bi (2%).

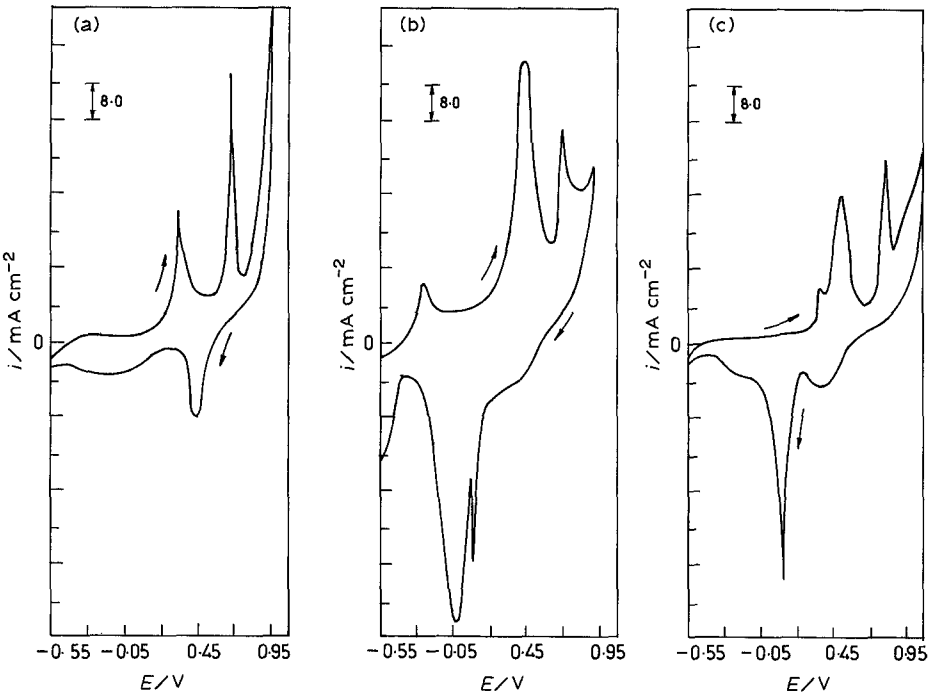

Fig. 5. The linear sweep cyclic voltammetric curves in argon saturated 1 M KOH solution at 25 °C and at 10 mV s^{-1}; (a) Ag–Sb (2%); (b) Ag–Bi (2%); (c) Ag.

with Reaction 2 being the overall processes for the formation of Ag_2O [9].

The curve for the Ag–Bi electrode (Fig. 5) has three anodic peaks with E_p values −0.325, 0.4 and 0.675 V and four cathodic peaks with E_p values 0.25, 0.1, 0.0 and −0.8 V. The curve corresponding for the Ag–Sb electrode (Fig. 5) has two anodic peaks with E_p values 0.3 and 0.625 V and two cathodic peaks with E_p values 0.425 and −0.175 V (broad and diffused). Similar curves obtained in the extended potential range from −1.3 to 1.1 V, covering hydrogen evolution on the Ag–Sb (2%), Ag–Bi (2%) alloys and on bismuth (pure) and antimony (pure) are shown in Fig. 6.

The salient features of the cyclic voltammetric curves obtained on these electrodes are as follows:

(i) The anodic peak at 0.50 V observed at Ag–Bi is absent for Bi.
(ii) The small peak at 0.35 V observed on Ag is broader on Ag–Bi.
(iii) The broad peak at 0.2 V observed on Sb is absent at Ag–Sb.
(iv) The additional anodic peaks at 0.3 and 0.625 V on Ag–Sb are absent on Sb.
(v) The additional anodic peak at 1.05 V on Sb is absent on Ag–Sb.

An analysis of these results reveal that the anodic peak at 0.50 V in the cases of Ag, Ag–Bi and Ag–Sb, can be assigned to the oxidation of silver. The broadening of the small peak at 0.35 V on Ag–Bi can be attributed to the kinetic hindrance offered by the Bi_2O_3 film to the initial oxidation of silver. The anodic peak at 0.220 V obtained on antimony corresponds to the Sb/Sb_2O_3 redox process [9]. The anodic peak at 0.625 V on Ag–Sb has been assigned to the oxidation of silver. The additional anodic peak at 1.05 V on

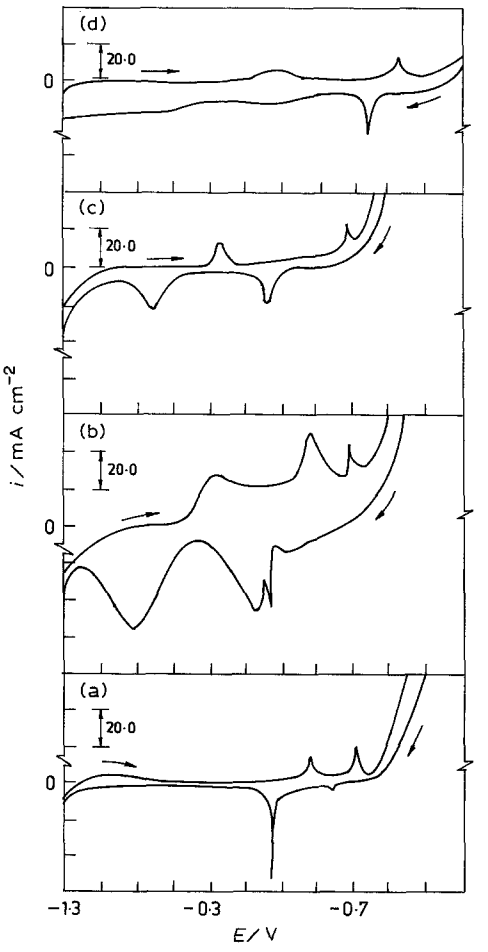

Fig. 6. The linear sweep cyclic voltammetric curves in argon saturated 1 M KOH solution at 25 °C and at 10 mV s^{-1}; (a) Ag–Sb (2%); (b) Ag–Bi (2%); (c) Bi; (d) Sb.

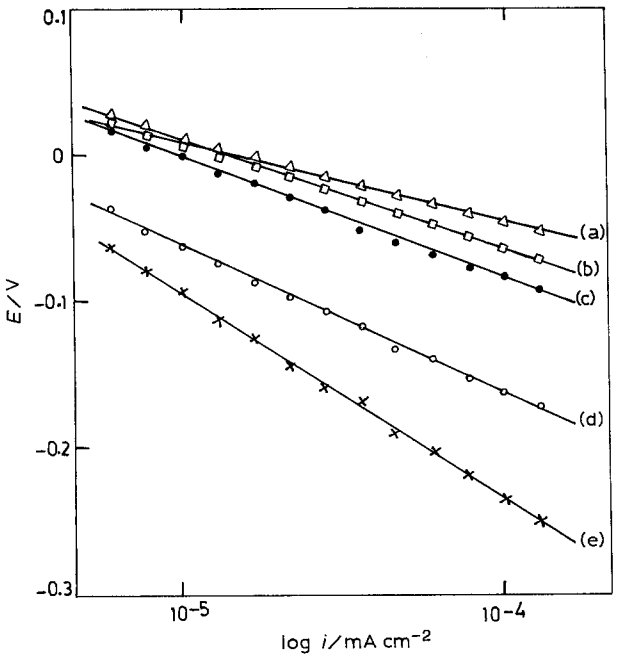

Fig. 7. The E against log i plots for the oxygen reduction reaction in 1 M KOH at 1200 r.p.m. and at 28 °C; (a) Ag–Sb (2%); (b) Ag; (c) Ag–Sb (5%); (d) Ag–Bi (2%); (e) Ag–Bi (5%).

antimony is attributed to the oxidation of Sb_2O_3 to higher oxides of antimony [9].

The currents due to the evolution of oxygen observed beyond 1.0 V ranked in the following order:

$$\text{Bi} > \text{Ag–Bi} > \text{Ag–Sb} > \text{Ag}$$

The cathodic peaks on Ag–Bi and Ag–Sb electrodes at E_p values 0.25 and 0.0 V correspond to the dual reduction stages of AgO to metallic Ag. The other peaks with E_p values 0.1 V (Bi and Ag–Bi), 0.8 V (Ag–Bi) and −0.725 V (Bi) correspond to the reduction processes of Bi_2O_3 to Bi(OH) and then to metallic Bi. The cathodic peaks having E_p values 0.8 and 0.220 V on Sb are attributed to the reduction processes of antimony oxides to metallic Sb. The apparent anomalies observed in the E_p values on the present electrodes, compared with those of Ag or Bi or Sb, are attributed to the co-existence of these composite oxides on the electrode surfaces.

3.6. *Oxygen reduction kinetics*

As Ag–Bi/Sb electrodes have shown extreme stability in the oxygen reduction potential region, and silver is a well known electrocatalyst [4, 5, 10–12], a knowledge of its catalytic activity with co-existing Sb or Bi (although not in an alloy form) is of interest. Therefore, initially, the present set of alloy electrodes were investigated under potentiostatic steady state polarization conditions for the oxygen reduction reaction in oxygen saturated 1 M KOH solution at a constant rotation speed of 1200 r.p.m. The E against log i plots obtained for the oxygen reduction reaction on these electrodes are shown in Fig. 7. The steady state kinetic data derived from these results are presented in Table 3. The magnitude of the Tafel slope values (RT/F) indicates that the oxygen reduction

Table 3. Steady-state kinetic data for the oxygen reduction reaction on Ag–Bi/Sb electrodes in 1 M KOH at 1200 RPM and at 28°C

Electrode system	*Tafel slope b* ($mV\,sec^{-1}$)	*Equilibrium exchange current density* i_0 ($10^7 \times A\,cm^{-2}$)
Ag–Sb (2%)	55	2.0
Ag	85	7.0
Ag–Sb (5%)	86	6.5
Ag–Bi (2%)	50	4.5
Ag–Bi (5%)	135	6.0

kinetics on these electrodes is controlled by the diffusion of the dissolved oxygen from the bulk to the electrode surfaces. Moreover, the transfer of the second electron to the adsorbed oxygen is the rate determining step of the oxygen reduction. The effect of rotation on the oxygen reduction currents is shown in Fig. 8. It becomes evident that the oxygen reduction kinetic currents vary significantly as a function of the rotation speed of the electrode. This also suggests the dependence of the kinetics on the diffusion of oxygen.

The cyclic voltammetric curves obtained in the oxygen reduction potential region at slow sweep rates on Ag–Bi/Sb electrodes are shown in Fig. 9. From a comparative analysis of both the steady state and the cyclic voltammetric data on the oxygen reduction behaviour of these electrodes, they rank in the following order:

$$\text{Ag–Sb (2\%)} > \text{Ag} > \text{Ag–Sb (5\%)} > \text{Ag–Bi (2\%)}.$$

Further, it becomes obvious from these results that the oxygen reduction process commences only at −0.1 V with a wave form and attains limiting currents at −0.4 V. The above trend in their activity is attributed to the synergistic effects. The effect of sweep rate on the observed currents in the cyclic voltammetric curves for Ag–Sb (2%) electrode is shown in Fig. 10.

The effects of activities of the KOH solutions and that of temperature on the oxygen reduction currents obtained on the Ag–Sb (2%) electrode are shown in Fig. 11. Increasing sweep rates increase the oxygen reduction currents. The higher the sweep rate, the smaller is the negative potential at which the oxygen

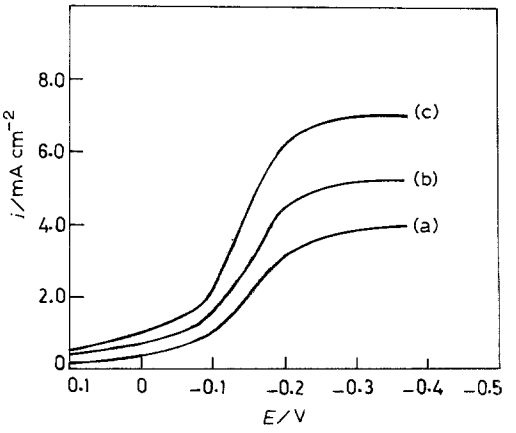

Fig. 8. The effect of rotation on the oxygen reduction currents on Ag–Sb (2%) electrode in 1 M KOH at 28 °C; (a) 600 r.p.m.; (b) 900 r.p.m.; (c) 1200 r.p.m.

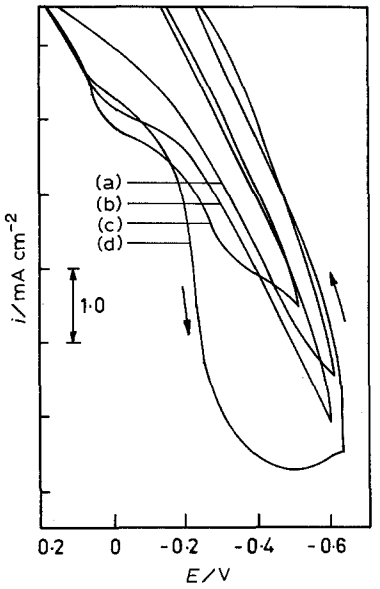

Fig. 9. The linear sweep cyclic voltammetric curves for the reduction of dissolved oxygen in 1 M KOH at 25 °C; (a) Ag–Bi (2%); (b) Ag–Sb (5%); (c) Ag; (d) Ag–Sb (2%).

reduction starts. The oxygen reduction currents are greater in 1 M than in 6 M KOH solution. Similar behaviour has been reported to occur at pure silver electrodes [13,14] and this has been attributed to the lower solubility of oxygen in 6 M than in 1 M KOH. The effect of temperature on the oxygen reduction currents is very little. At elevated temperatures, the oxygen reduction wave is initiated at less negative potentials.

4. Conclusions

(i) The various stages of electrochemical formation of oxide layers on Ag–Bi/Sb alloy electrodes when compared with electrodes of pure Ag, Bi and Sb are reported for the first time.
(ii) Oxygen reduction currents on these electrodes rank in the order:

Ag–Sb (2%) > Ag > Ag–Sb (5%) > Ag–Bi (2%).

(iii) The surfaces of the electrodes became rough after

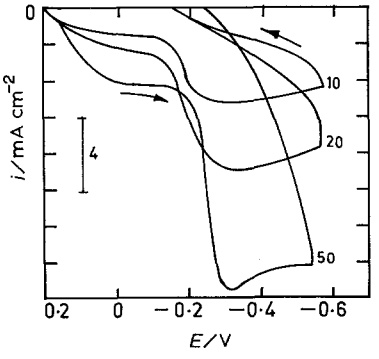

Fig. 10. The linear sweep cyclic voltammetric curves for the reduction of dissolved oxygen in 1 M KOH at 25 °C on Ag–Sb (2%) electrode at 10, 20, 50 mV s^{-1}.

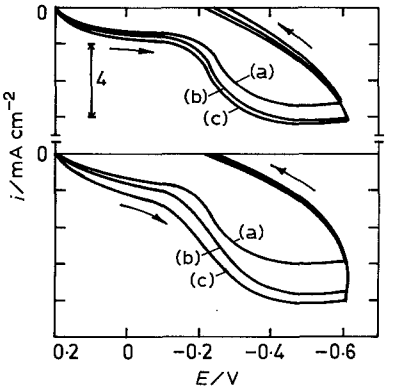

Fig. 11. The linear sweep cyclic voltammetric curves for the reduction of dissolved oxygen in KOH solutions at 10 mV s^{-1} and at 25 °C. Upper sweep – effect of concentration of KOH: (a) 6, (b) 3 and (c) 1 M. Lower sweep – effect of temperature: (a) 25, (b) 60 and (c) 80°C.

cathodic reduction of the oxides. Evolution of hydrogen leads to further roughening of the electrode surfaces.
(iv) The oxygen evolution currents on these electrodes rank in the order:

Bi > Ag–Bi (2%) > Ag–Sb (2%) > Ag.

Acknowledgement

The authors are thankful to the Director, CECRI, Karaikudi, for his kind encouragement and permission to publish this paper.

References

[1] B. V. Tilak, R. S. Perkins, H. A. Kozlowska and B. E. Conway, *Electrochim. Acta* **17** (1972) 1447.
[2] N. A. Hampsen, K. J. McDonald and J. B. Lee, *J. Electroanal. Chem.* **45** (1973) 147.
[3] J. Ambrose and R. G. Barradas, *Electrochim. Acta* **19** (1974) 781.
[4] E. W. Justi and A. W. Winsel, *J. Electrochem. Soc.* **100** (1961) 1073.
[5] P. K. Adanuvor and R. E. White, *J. Electrochem. Soc.* **135** (1988) 2509.
[6] M. Brezina, J. Koryata and M. Musilova, *Coll. Czeck, Commun.* **33** (1968) 3367.
[7] R. Chandrasekaran, S. Deenadayalan and V. K. Venkatesan, in 'Advances in Electrochemical Science and Technology', The SAEST (edited by K. I. Vasu), Oxford and IBH Publishing Company, New Delhi (1988) pp. 251–9.
[8] D. T. Hawkins and R. Hultgren, in 'Metals Hand Book', 8th edn, Vol. 8 (edited by Taylor Lyman), American Society of Metals (1973) pp. 252 and 254.
[9] J. P. Hoare, in 'Encyclopedia of Electrochemistry of the Elements', Vol. 2 (edited by A. J. Bard), Marcel Dekker, New York (1974) pp. 191–382.
[10] M. R. Tarasevich, R. C. Burstein and Yu. A. Chiemadzhev, in 'Fuel Cell Systems II' (Advances in Chemistry Series), (edited by Robert E. Gould), ACS Publication, Washington DC (1969) p. 81.
[11] S. Z. Beer and Y. L. Sandler, *J. Electrochem. Soc.* **112** (1965) 1133.
[12] A. W. Czanderna, *J. Phys. Chem.* **68** (1964) 2765.
[13] Keith E. Gubbins and Robert D. Walker Jr., *J. Electrochem. Soc.* **112** (1965) 469.
[14] T. Hurlen, Y. L. Slander and E. A. Pantier, *Electrochim. Acta* **11** (1966) 1463.